Journal of Urban Management and Energy Sustainability (JUMES)

Homepage: http://www.ijumes.com

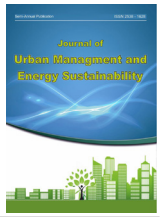

CASE STUDY RESEARCH PAPER

Construction of a device for laboratory investigation of seepage specifications in different states of the Karkheh dam dam-wall

Ali Mahbod[1*], Hamid Reza Saba[2], Mostafa Yousefi Rad[3], Hamid Lajvardi[4]

1 Department of civil , Faculty of Earth Sciences , Islamic Azad University , Arak , Iran*
2 Assistant professor , Department of Civil Engineering, Tafresh University , Iran
3 Department of Geology , Faculty of Earth Sciences , Arak University of Technology , Iran
4 Department of Civil , Faculty of Earth Sciences, Islamic Azad University , Arak , Iran

ARTICLE INFO

Article History:
Received 2024-09-05
Revised 2024-11-17
Accepted 2024-12-26

Keywords:
Earth dam, geotechnical, percolation test, Plaxis, water retaining wall

ABSTRACT

Earthen dams, as one of the largest earthen structures, are exposed to various failure mechanisms, some mechanisms such as cracking and hydraulic failure are created in the body of the dam, and some other mechanisms such as liquefaction, divergence and dissolution are caused by the characteristics of Geotechnical is the foundation of the region. In this research, studies were conducted to evaluate geomechanical parameters effective in the occurrence of hydraulic failure and to understand the interaction of the dam body with these parameters and to provide a safe model to reduce the risk of building earthen dams and to study how to deal with problematic foundations. Modeling of the problem was done with finite element numerical method using PLAXIS computing code. In this laboratory, by changing the mixing percentage of the dam wall materials, their effect on the behavior of the earthen dam was studied. The results showed that the laboratory results presented in this research have a good overlap with the results of the software and by using this device, it is possible to calculate the amount of seepage in each mixing design according to the dimensional analysis.

DOI: 10.22034/ijumes.2024.2043838.1263

Running Title: Laboratory investigation of seepage specifications in different states of the Karkheh dam

NUMBER OF REFERENCES	NUMBER OF FIGURES	NUMBER OF TABLES
26	26	04

*Corresponding Author:
Email: *alimahbod@yahoo.com*
Phone: *+98988634132451*
ORCID: https://orcid.org/0009-0008-9959-9549

INTRODUCTION

Usually, excessive seepage should be prevented behind earth dams. Using the plastic concrete dam wall technique reduces seepage through the dams. Also, the dam wall as a part of the dam must have appropriate flexibility in addition to maintaining stability. In this study, a non-homogeneous earth dam was studied numerically. This dam is located on a foundation with non-homogeneous layers. Various modeling was performed with Plaxis software. By changing various parameters, their effects on the dynamic behavior of the dam were examined. According to the obtained values, a mixture of one cubic meter of concrete with an internal friction angle of 18 degrees, adhesion of 1500 kPa and Young's modulus of 1500 MPa is recommended; these values are based on the maximum displacement of the dam wall without rupture and according to the parametric changes made to the input parameters under study. (Rahimi, 2010) The panel method is used to construct retaining walls with plastic concrete or structural concrete materials. The consequence of this method is that due to the erosion of its materials, the acceptable performance of the wall as a seepage control is questioned. (Hu et al., 2010)(Du et al., 2014a) Vertical soil-bentonite retaining walls installed with the dug-in Goodgal technology are widely used as in-situ barriers in the United States, Canada, and Japan to control the movement of subsurface contamination. The effects of fines content, bentonite content, and sand grading and the type and amount of modification (such as zeolite and activated carbon) on permeability and hydraulic conductivity (k) have been extensively studied, as have the relationships between permeability and lateral resistance of sand/bentonite (SB sand) and sand/clay (SC) soil embankments. (Du et al., 2015)(Du et al., 2014b)(Xue et al., 2013) Soil-bentonite embankments usually have an undrained shear strength of less than 10 kPa due to their relatively high moisture content, and in the presence of external loads, the strength is one of the main design parameters. (Evans et al., 1995)(Sharma and Reddy, 2004)(Horpibulsuk et al., 2007) Studies show that, compared to old sand-soil, clay SB embankments with a moisture content of 5 to 15%, they perform well in terms of compressibility and hydraulic conductivity. A significant increase (e.g. 4 to 10 times) in hydraulic conductivity may also occur, which may lead to failure in case of contact with chemical fluids, to meet the specific monitoring limit of 10^(-9) m/s for sand-sand SB and NA-bentonite embankments. (Fan et al., 2014a)(D,Appolonia, 1980) Changes in the engineering properties of engineered soil barriers can be attributed to: (1) shrinkage of the bentonite particle dispersion double layer due to increased pore water metal concentrations, (2) breakdown of carbon bonds or cementation between clay particles due to acid corrosion, and (3) complex geochemical and mineral changes.(Malusis and McKeehan, 2013) (Yong et al., 2009) Previous studies have shown that initial moisture content can have a significant effect on clean and contaminated clay SB embankments as well as disturbed natural clay. (Grim, 1968)(Yukselen et al., 2013)

With increasing mean effective vertical compaction stress, the consolidation coefficient increases slightly, which is consistent with the reported -Na bentonite/old sandy soil embankments. (Taylor, 1948)(Sivapullaiah et al., 2006) It is mainly controlled by the excess pore pressure loss rate. In addition, the increase in cv with increasing mean effective vertical stress is due to the larger change in mv, in terms of , compared to the hydraulic conductivity. (Xu et al., 2012)(Li, et al., 2013b)Such an observation has also been reported in previous studies for Na-bentonite/old sandy soil embankments, activated carbon-modified -Na bentonite/sandy soil embankments, and zeolite-modified -Na bentonite/sandy soil embankments. (Evans et al., 1995) Fils (1996) and Roffing et al. (2010) suggested that the lateral soil pressure acting on a soil-bentonite embankment can be much lower than the geostatic pressure, which is estimated to be less than 100 kPa based on a modi-

fied lateral pressure model (Mishra et al., 2009). There is a threshold concentration, beyond which the effect of Pb or Ca concentration on the change in hydraulic conductivity is negligible. The threshold Pb or Ca concentration of the embankment presented here and the SB sand embankment reported by Malosis and McKeehan (2013) varies from 500 to 130 mmol/l, depending on the bentonite content . (Ruffing et al., 2010)The range of hydraulic conductivity ratios of SB sand embankments reported by Malosis and McKeehan (2013) varies from 3.5 to 16. The possible reasons for this discrepancy are: (1) the hydraulic conductivity of the embankments in this study was calculated based on the one-dimensional consolidation theory of Terzaghi, (2) the clay SB embankments tested here were prepared by mixing a mixture of clay (kaolin)-Ca-bentonite with a Pb(NO3) solution, and (3) in this study, -Ca bentonite was used, while Malosis and McKeehan used Na-bentonite. (Malusis and McKeehan, 2013) According to the Goy-Chapman theory (Mitchell and Suga, 2005), with increasing Pb concentration, the degree of contraction of the double dispersing layer or the reduction of the swelling potential of bentonite will increase, which will reduce the condensation limit and increase the hydraulic conductivity of bentonite, as suggested by Asridharan et al. (2007) and Horpibolski et al. 2011. (Grim, 1968) The problem was modeled using the finite element numerical method using the PLAXIS computational code. In this numerical study, by changing important parameters including the internal friction angle, adhesion, and Young's modulus, their effects on the dynamic behavior of the dam were investigated. During this process, by discarding the cases that were broken in the modeling, the stability of the dam was ensured in all cases and results. The Plaxis outputs, including the total displacement change in the dam wall, the change in mesh, and the change in pore water pressure in the entire dam body and in the dam wall, were examined to consider the effect of all influential factors on the flexibility conditions of the dam's dam wall. To validate the numerical modeling, the results obtained were compared with the actual values taken from the Karkheh Dam, and then, in order to obtain suitable conditions including the highest flexibility, lowest pore water pressure, and the finest mesh, the results were presented as a percentage of the required change in materials. The flexibility of the water retaining wall was considered as a criterion for flexibility based on the maximum displacement of the water retaining wall without rupture, and the optimal material composition of one cubic meter of concrete was proposed. Due to the time-consuming nature of numerical modeling for developing models, a program was designed in Matlab that calculates each of the output values based on the input values. Then, an active graph is drawn for each of the outputs. The error percentage of the program is within acceptable limits.

Introduction to the dam under study:

The Karkheh earthen dam has a clay core, a maximum width at the base of 1100 meters and at the dam crest of 12 meters, the length of the dam crest is 3030 meters, the height of the crest from the base is 127 meters, and the total volume of the reservoir is 3.7 billion cubic meters.(Hong et al., 2012) Its construction site is made of heterogeneous layers of Bakhtiari conglomerate, the mechanical properties of the layers are not the same in different directions, and its calcareous cementation is not complete, and it has open sandy channels and relatively high permeability. There are layers of lichen and sand lenses with very low permeability between the conglomerate layers. The Karkheh conglomerate contains 45% chert and silica and is highly abrasive. One of the important features of the Karkheh conglomerate is its high permeability and low injection ability in order to control seepage from the dam base. Due to this feature of the conglomerate, after conducting an injection test in the study phase and failing to create a unified watertight curtain and a slight decrease in permeability after injection, the wa-

tertight wall option was selected and designed instead of injection. The Karkheh Dam dam is 2940 meters long, 18 to 78 meters deep, 80 to 100 centimeters thick, and has a total area of 162,000 m^2. It is made of plastic concrete and cast using the thermal method. The axis of the dam dam is aligned with the dam axis and a clay core is created in the middle. (Mishra et al., 2009)In the middle sections of the dam, the dam dam is connected to one of the clay layers, and in the side sections, parts of the wall are suspended in the conglomerate layer.

Numerical modeling:

Considering the use of Plaxis computational code, in this research work, in order to ensure the accuracy of the outputs and verify the method used, an earth dam whose dynamic analysis results are available in a reliable source was modeled and the accuracy of the results was examined. In order to ensure the accuracy of the outputs and eliminate any possible errors, the Karkheh earth dam was selected, which has been previously analyzed by Tabrei and Abrishmi (2018). Considering that the maximum height of the Karkheh dam is 127 meters, the maximum stress and pressure applied to the dam wall occurs at this section. Also, the dam wall conditions at this section pass through various conglomerate and clay layers and there are layer-by-layer foundation conditions around it, the said section was considered as the basis for static and dynamic analyses. In the studied section, 8 meters of the dam wall is sunk into the clay core and after passing through the layers of conglomerate-1, loam-1, and conglomerate-2, it is sunk 2.5 meters into the loam-2 layer. At the contact point of the clay core with the conglomerate foundation, a plastic concrete reinforcement trench with a maximum width of 14 meters, a minimum width of 8 meters, and a thickness of 1.5 meters has been constructed. For the purpose of simulation, the largest cross-section of the dam is simulated in plane strain using 15-node triangular elements and the interface of the dam wall and foundation is simulated using joint elements. The first dam intake was selected as the static critical loading and static stress-strain analysis was performed. In order to simulate the problem, an earthen dam with a clay core with a crest width of 10 meters and a height of 100 meters was modeled. For the downstream of the dam, a zero head elevation was assumed to be flush with the ground surface downstream of the dam body. The upstream head of the dam was calculated based on the freeboard calculated at the bottom and the height of the dam crest (Formula 1). Due to the lack of necessary information on wind speed, a wind speed of 160 km/h was assumed according to the USBR regulations. Also, the fetch length was assumed to be 20 km and the average depth of the reservoir was assumed to be 25 m. Also, the upstream wall of the dam body was assumed to be riprap, which multiplies the wave effect by 1.5. A schematic of the external characteristics of the modeled dam is presented in Figure 1. (Fig. 1)

The specifications of the materials used in the modeling for a 60-meter-thick rock foundation with a specific gravity of 40 kPa, a cohesion of 100 kPa, and an internal friction angle of 75 degrees are presented in Table 1. The geotechnical specifications of the materials used in the modeling are also presented in Table 1. (Tab. 1)

In order to provide a complete analysis of the water retaining wall, the material parameters and characteristics of the water retaining wall must be evaluated within a reasonable range. Therefore, the maximum range of variations in the material characteristics of the water retaining wall is determined and presented in Table 2. (Tab. 2)

The displacement diagram of the dam's watertight wall in numerical modeling and studies by Tabrei and Irishmi (2017) is presented in Figure 2. Comparison of the results shows that the results from the validation have a similar trend, although with a slight difference compared to the Tabrei model. (Fig. 2)

$$Free\ Board = 1.5 \times \left(0.032\sqrt{F.V} + 0.76F^{0.25} + \frac{V^2 F.cosA}{63000D} \right)$$

$$Free\ Board = 1.5 \times \left(0.032\sqrt{20.160} + 0.76 \times 20^{0.25} + \frac{160^2 \times 20}{63000 \times 25} \right) = 3.5m$$

$$Free\ Board \approx 4m$$

$$Up\ stream\ Head = 98.5 - 4 = 94.5\,m$$

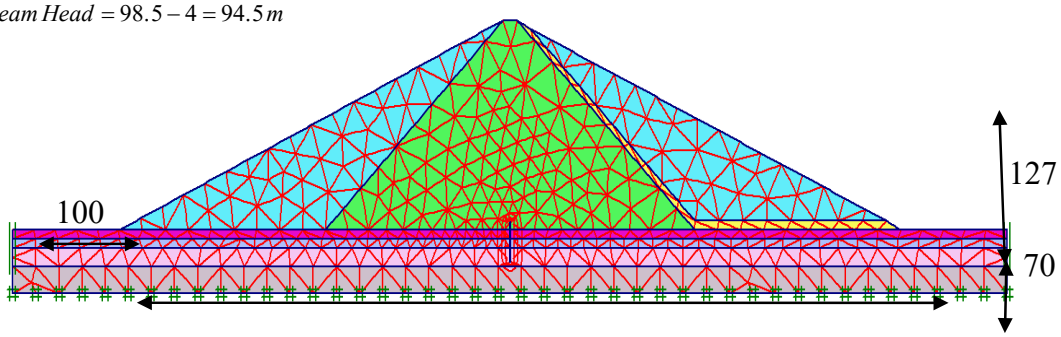

Figure 1: Details of Dam and Waterproof Wall model, waterproofing and meshing in the study section

Table 1: Geotechnical specifications of materials used in modeling

Soil type	E (kN/m²)	C (kN/m²)	ø	K (m/day)
shell	5500	30	35	0.2
the core	2500	60	30	.001
foundation soil	3500	1	33	0.4
drain	30,000	1	35	10
Cut off wall	4000	1	33	0.05

Table 2: Range of variations in the characteristics of waterproof wall materials

Soil type	Special Weight (kN/m²)	ø	Relative density (percentage)	SPT
Sand loose	18.1<G<16.6	33<Ø <29	Dr<35	10<N<4
Sand medium	19.3<G<18.1	38< Ø <33	<Dr<65 35	30<N<10
Sand dense	20.4<G<19.3	40< Ø <38	<Dr<85 65	50<N<30
Soil type	Special Weight (kN/m²)	Adhesion (kN/m²)	e50	SPT
clay soft	17.8<G<15.1	21<C <4	1.65<e<4.38	4<N<1
clay medium	20.2<G<17.8	57< C <21	0.9<e<1.65	10<N<4
clay stiff	20.8<G<20.2	94< C <57	0.66<e<0.9	16<N<10
clay very stiff	21.5<G<20.8	194< C <94	0.43<e<0.66	32<N<16
Soil type	Special Weight (kN/m²)	Adhesion (kN/m²)	ø	SPT
Silt medium	20.2<G<17.9	29<C <10.4	30<Ø <27	10<N<4
Silt stiff	20.8<G<2.0.2	47< C <29	32< Ø <30	16<N<10
Silt very stiff	21.5<G<2.8	96< C <47	35< Ø <32	32<N<16

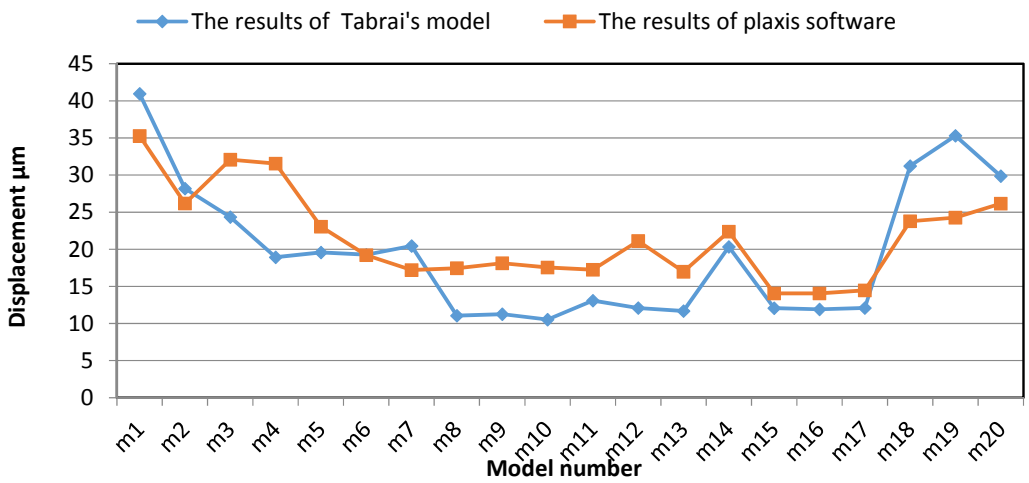

Figure2: Diagram of the displacement of the dam's watertight wall in numerical modeling and Tabrei and Sarishmi studies (2018)

MATERIALS AND METHODS

Modeling and analysis process

The analyses were started with an initial investigation and identification of critical points. In the initial investigation, the three parameters of internal friction angle, adhesion and Young's modulus were changed separately within a certain range, keeping the other parameters constant. In order to examine carefully and select critical points, the range of internal friction angle was selected from 0 to 50 degrees, adhesion from 1 kPa to 2000 kPa and elastic modulus from 100 MPa to 2000 MPa. In Plaxis software, medium meshing was used and for greater accuracy, the meshing was made finer around the dam wall. The best flexibility of the dam wall was considered as maximum deformation in the dam wall without causing rupture in it. For this purpose, models in which rupture occurred were excluded from the investigations. Also, for greater certainty, the maximum change in the form of elements in the entire dam body was also examined.

Modeling with Plaxis:

The final models were made with the specifications and assumptions assumed in the initial study and only with rotational changes in the three parameters under study. Pore water pressure will have an inverse effect on effective stress, which is why it is necessary to study this factor. Therefore, this factor will be studied in the dam body and the dam wall in the following. (Fig. 3)

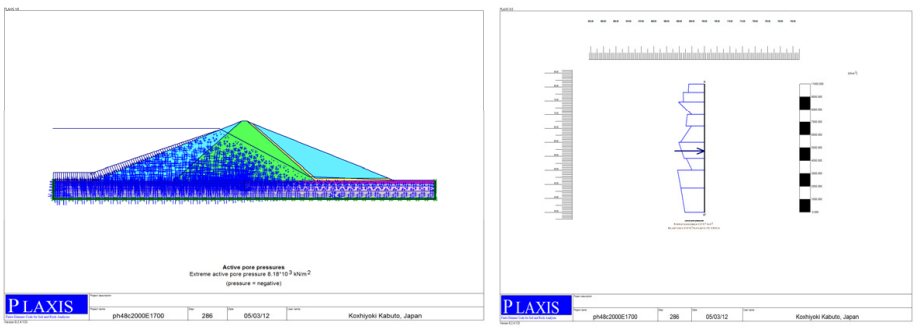

Figure 3: Checking pore water pressure

The above figures indicate the position and conditions such as the pore water pressure, the position of the water surface, and the phreatic line in the entire dam. They also provide the pore water pressure profile in the dam wall under conditions of changing Poisson's ratio, internal friction angle, and adhesion while keeping other conditions constant. The results are then analyzed.

DISCUSSION AND FINDINGS

Final Analysis Summary

According to the study conducted by Plaxis, which was fully reviewed in the previous section, the results can be reviewed as follows. (Tab. 3)

Table 3: Final GPA Results

Sample number	pore pressures (Cut off)	pore pressures (Dam)	Concrete specifications			Sample number	pore pressures (Cut off)	pore pressures (Dam)	Concrete specifications		
			Phi	C	E				Phi	C	E
64	2.31	7.3	22	1500	1500	1	2.64	4.38	0	1300	100
65	2.57	7.87	22	1500	1700	2	2.47	5.47	0	1300	800
66	3.03	5.09	22	1900	100	3	2.51	5.67	0	1300	1300
67	4.36	5.17	22	1900	800	4	2.83	6.05	0	1300	1500
68	3.41	6.98	22	1900	1300	5	2.48	3.13	0	1300	1700
69	3.78	7.61	22	1900	1500	6	2.65	4.73	0	1400	100
70	4.05	8.19	22	1900	1700	7	2.75	5.56	0	1400	800
71	2.74	5.13	22	2000	100	8	3.29	5.89	0	1400	1300
72	3.14	5.17	22	2000	800	9	2.8	6.01	0	1400	1500
73	2.82	6.98	22	2000	1300	10	2.88	6.2	0	1500	1700
74	3.48	7.59	22	2000	1500	11	3.08	4.93	0	1500	100
75	2.39	8.22	22	2000	1700	12	3.2	5.88	0	1500	800
76	2.9	5.09	24	1300	100	13	2.96	6.04	0	1500	1300
77	2.71	5.2	24	1300	800	14	3.27	6.27	0	1500	1500
78	2.82	6.8	24	1300	1300	15	4.22	6.38	0	1500	1700
79	2.34	7.23	24	1300	1500	16	3.03	5.13	0	1900	100
80	2.77	7.53	24	1300	1700	17	3.03	5.15	0	1900	800
81	3.06	5.09	24	1400	100	18	3.37	6.75	0	1900	1300
82	4.82	5.19	24	1400	800	19	2.78	7.08	0	1900	1500
83	2.35	6.89	24	1400	1300	20	2.38	7.35	0	1900	1700
84	2.79	7.37	24	1400	1500	21	3.06	5.13	0	2000	100
85	3.01	7.75	24	1500	1700	22	2.49	5.2	0	2000	800
86	3.77	5.09	24	1500	100	23	2.75	6.81	0	2000	1300
87	2.68	5.18	24	1500	800	24	3.38	7.23	0	2000	1500
88	3.27	6.97	24	1500	1300	25	2.56	7.54	0	2000	1700
89	2.79	7.47	24	1500	1500	26	2.66	5.1	18	1300	100
90	3.02	7.98	24	1500	1700	27	2.46	5.16	18	1300	800
91	3.03	5.09	24	1900	100	28	2.54	6.6	18	1300	1300

Sample number	pore pressures (Cut off)	pore pressures (Dam)	Concrete specifications			Sample number	pore pressures (Cut off)	pore pressures (Dam)	Concrete specifications		
			Phi	C	E				Phi	C	E
92	2.45	5.17	24	1900	800	29	2.51	6.87	18	1300	1500
93	3.55	6.98	24	1900	1300	30	2.61	7.13	18	1300	1700
94	3.57	7.6	24	1900	1500	31	3.06	5.09	18	1400	100
95	3.44	8.21	24	1900	1700	32	3.23	5.18	18	1400	800
96	3.06	5.09	24	2000	100	33	2.85	6.76	18	1400	1300
97	2.57	5.17	24	2000	800	34	2.52	7.12	18	1400	1500
98	3.29	6.98	24	2000	1300	35	2.36	7.39	18	1500	1700
99	2.69	7.58	24	2000	1500	36	2.9	5.09	18	1500	100
100	2.3	8.21	24	2000	1700	37	2.94	5.2	18	1500	800
101	2.99	5.09	48	1300	100	38	2.44	6.84	18	1500	1300
102	3.37	6.98	48	1300	800	39	2.39	7.3	18	1500	1500
103	2.37	7.58	24	1300	1300	40	2.83	7.62	18	1500	1700
104	2.29	7.58	24	1300	1500	41	3.02	5.09	18	1900	100
105	2.5	8.18	24	1300	1700	42	2.48	5.17	18	1900	800
106	3.03	5.09	24	1400	100	43	2.82	7.01	18	1900	1300
107	4.1	5.17	24	1400	800	44	5.88	7.59	18	1900	1500
108	3.23	6.98	24	1400	1300	45	2.42	8.13	18	1900	1700
109	2.35	7.58	24	1400	1500	46	3.01	5.13	18	2000	100
110	5.55	8.18	24	1500	1700	47	3.34	5.17	18	2000	800
111	3.78	5.09	24	1500	100	48	2.35	6.99	18	2000	1300
112	2.42	5.17	24	1500	800	49	2.34	7.62	18	2000	1500
113	2.6	6.98	24	1500	1300	50	2.79	8.16	18	2000	1700
114	6.31	7.58	24	1500	1500	51	2.75	5.09	22	1300	100
115	2.29	8.18	24	1500	1700	52	2.98	5.18	22	1300	800
116	3.03	5.09	24	1900	100	53	2.8	6.76	22	1300	1300
117	2.43	5.17	24	1900	800	54	2.5	7.11	22	1300	1500
118	4.04	6.98	24	1900	1300	55	2.93	7.39	22	1300	1700
119	3.64	7.58	24	1900	1500	56	3.03	5.09	22	1400	100
120	3.83	8.18	24	1900	1700	57	3.06	5.2	22	1400	800
121	2.7	5.09	24	2000	100	58	2.36	6.85	22	1400	1300
122	3.11	5.17	24	2000	800	59	2.99	7.31	22	1400	1500
123	2.39	6.98	24	2000	1300	60	3.32	7.63	22	1500	1700
124	2.34	7.58	24	2000	1500	61	3.03	5.09	22	1500	100
125	2.34	8.18	24	2000	1700	62	3.02	5.18	22	1500	800
						63	3.23	6.93	22	1500	1300

In-situ testing:

In addition to calculating the amount of water loss, the settlement analysis of the foundation of earth dams plays a fundamental role in calculating the amount of pore water and consequently in stability analysis. Also, any settlement analysis depends on the hydraulic properties of the materials constituting the dam. To investigate the effect of the hydraulic conductivity parameter on the settlement phenomenon, a laboratory model of an earth dam was built and investigated by accurately measuring the hydraulic parameters of the materials in saturated and unsaturated states. (Fig. 4)

Initially, in order to measure the required parameters and clarify the obstacles, an earthen dam model was implemented in natural ground. In this model, the necessary sealing was done using a pressure brick wall with cement plaster. Initial studies and modeling were carried out, but problems such as rainfall and changes in water level and the impossibility of controlling the internal environment of the device led to the decision to continue the device with glass and a metal frame. Moisture distribution in porous environments in the presence of permanent and non-permanent settlement flows In many issues, the theory of settlement from the foundation and body of an earthen dam, the interaction of surface water with groundwater, settlement and water loss from water transfer channels, various environmental issues, and studies of the spread and spread of pollution are of Interest. Many researchers have paid attention to settlement flows in unconfined environments with a free surface, and recently new methods have been proposed to analyze such issues. For example, the unsteady settlement flow affected by rainfall and water level fluctuations has been studied using the saturated-unsaturated settlement model based on the two-phase flow theory of air and water in porous media. The so-called extended pressure solution method was presented to solve the settlement problem with a free flow surface by using a single step function (Hoyside) 0 and 1. In recent years, with modifications to the Hoyside function condition, the extended pressure method has been effectively modified; so that the convergence of the settlement equation solution in unconfined conditions has improved significantly. Many of the presented models depend on water pressure or hydraulic head. As a result, in these numerical models and methods, due to the presence of the capillarity phenomenon, the water-air contact surface cannot be accurately determined. Also, due to the strong changes in the degree of soil saturation near this surface, it is difficult to determine the exact position of the phreatic surface. Therefore, to accurately determine the

Figure 4: Excavation and control of the dam model in the ground and the end of the earth dam plaster

position of the settlement surface and the practice line, it is necessary to know the hydraulic conductivity changes of the porous medium in the unsaturated state. In fact, the limitation of using settlement analysis models is related to determining the hydraulic properties of the environment, especially moisture changes and, consequently, changes in the permeability of the environment under unsaturated conditions. In this study, the effect of using unsaturated hydraulic properties of soil materials on the phenomenon of unconfined settlement of the earthen dam body was investigated. Accordingly, the location of the settlement line, water pressure distribution, and the amount of flow passing through the foundation body of a homogeneous earthen dam were studied.

Laboratory model:

In order to investigate the subsidence phenomenon in the body of earth dams, a laboratory model of a homogeneous earth dam with a height of 31.75 cm was built symmetrically with respect to the dam axis (scale of the constructed device 1: 400). In order to investigate the subsidence line and pore water pressure in the dam body, many piezometers with a distance of 10 to 15 cm and proportional to the dimensions were used in several rows. Considering the height of the dam, the heel width was calculated as 98.26. (The slope ratio of the dam is 1 to 1.5 and the width of the dam crest is 12 meters). Considering that it is desirable to conduct studies at a rate of 1.5 times the heel width, the dam foundation was assumed to be 147.39 cm on each side, so the device was ordered to be 4 meters long. The width of the device was assumed to be unity, and considering that the depth of the water retaining wall at its greatest part was 78 meters. The height of the device should be more than 51.25 cm, which was considered to be 151.25 cm, including the one-meter bases, but due to the comprehensiveness of the device, a net height of 2 m was considered in the construction. The device was made of framed glass to allow for peripheral inspection. These frames were considered vertical, which caused the pressure on each glass frame to be equal and made it possible to inspect at height. In addition, considering that the width of the frames was calculated to be about 90 cm, by making several holes in the glass in the horizontal direction to install the piezometers, the distance between the piezometers was assumed to be less than 15 cm. Also, this distance in the vertical direction (in three rows) was limited to the same 15 cm. According to the designed device, piezometers were installed at all points of the dam sample body with 15 cm grid intervals. In addition to being used as a piezometer, this process can also be used to calculate the outlet flow rate of each pore, which is one of the strengths of the designed device. The materials used in laboratory modeling were prepared exactly like the Karkheh Dam, which was Bakhtiari conglomerate, and according to the grain size curve and dimensional analysis and using the results of the Iranian soil mechanics government tests conducted in the Markazi province region, suitable and similar soil was identified and used as the foundation. Other dam specifications are assumed to be the same as the Karkheh Dam specifications, but because the subject of this thesis is the dam foundation and, of course, changes in the water wall, the dam body was implemented as a homogeneous dam. (Fig. 5)

Figure 5: Simulated soil of the Karkheh Dam foundation (in terms of specifications)

In the bottom section of the model, a rough surface plate was used to reduce the seepage flow at the point where the soil contacts the model body. Also, to reduce the seepage at the point where the side walls of the model and the

soil contact, a layer of fine sand was glued to the surface of the side walls. In addition to reducing the settlement flow at this level, this increases the friction between the soil and the surface of the model wall and prevents the phenomenon of soil and side plates separating from the model. The side plates of the model were made of plexiglass and the other parts were made of steel. On both upstream and downstream sides of the dam, water tanks with the ability to control the water level were considered to investigate non-permanent settlement conditions in the model.

Physical model body specifications and testing process

In any settlement phenomenon, in addition to the geometry and prevailing boundary conditions, material specifications play a major role in the formation and flow pattern. For the physical model of the Karkheh Dam, soil with a simulated grain size of Bakhtiari conglomerate containing a small percentage of silt was used. And in the dam body, the existing mixture with the dam grain size was used. The reason for using such materials is their rapid response to changes in boundary conditions and consequently saving time. To build the dam body, soil layers were poured to a thickness of 5 cm and compacted with a hand roller. Permeability measurement tests were performed after the settlement tests were completed. Since in the stability analysis and design of earthen dams, a non-permanent analysis is generally performed for the sudden drop in water level, non-permanent leakage tests are also performed in this case, non-permanent leakage tests were also performed in this case. Also, the amount of leakage passing through the dam body at the outlet of the laboratory model was measured in weight. Given that the main objective of this research is to study the effect of hydraulic parameters of the dam body and foundation materials by changing the characteristics of the water retaining wall on the leakage analysis of the earthen dam body (Karkheh), for this purpose, multiple piezometers were used to determine the amount of pore water pressure in the entire foundation and body of the dam.

Governing equations

The amount of volumetric moisture depends on the changes in the stress state and physical properties of the soil. This equation is usually solved by one of the finite element or finite difference numerical methods. Since the aim of this research was to investigate the effect of transfer functions including hydraulic conductivity and moisture characteristic curve in numerical modeling of the seepage problem in the Karkheh earth dam, and considering different types of flow in steady and unsteady states, the results were examined according to different states and presented based on the combination of different Conditions and functions. Considering that the earth dam body was built in 5 cm layers, the asymmetry in the hydraulic conductivity parameter of the body was obvious. In order to determine the ratio of horizontal to vertical hydraulic conductivity, considering the data obtained from the seepage test from the body and the dam foundation at the maximum water level

Figure 6: Transparent chamber of the earth dam model and the water retaining wall formwork

upstream (18 cm) and in steady and unsteady conditions, the model was calibrated based on the asymmetry of the hydraulic conductivity of the body. The reason for choosing this level was to accurately simulate the Karkheh dam. (Fig. 6)

Watertight wall

The prepared mold was prepared exactly equal to the width of the device and the height of 19.5 cm and the thickness of one cm. Rabits sheets were used to repair the watertight wall. The mixing plan of the plastic concrete of the watertight wall, including the combination of water, cement, granular materials and bentonite, was prepared according to the mixing plan of the previous experiments (determining the compressive strength) according to the table below and poured into the molds.

Table 4: Mixing plan specifications for watertight wall samples

Sample number	Adhesives	Bentonite	Cement
1	292.5	29.25	163.25
2	341.25	34.125	307.125
3	390	39	351
4	292.5	58.5	234
5	341.25	68.25	273
6	390	78	312
7	292.5	87.75	204.75
8	341.25	102.375	238.875
9	390	117	273
10	292.5	117	175.5
11	341.25	136.5	204.75
12	390	156	234
13	292.5	146.25	146.25
14	341.25	170.625	170.625
15	390	195	195
16	292.5	175.5	117
17	341.25	204.75	136.5
18	390	234	156

After the final setting of the plastic concrete, the dam wall blades were placed in place and the dam body was created on top of it, and then the test device was drained.

Figure 7: Placing the retaining wall under the dam model

RESULT AND CONCLUSION

In this series of experiments, dam walls were prepared according to the mixing plan mentioned above and two parameters of pore water pressure in the body and foundation of the dam as well as the outlet flow rate were studied. The amount of water leakage from the dam (water transferred from upstream to downstream) was measured at the end of each day. For example, in the case of dam wall number one, the leakage rate is as shown in the graph below.

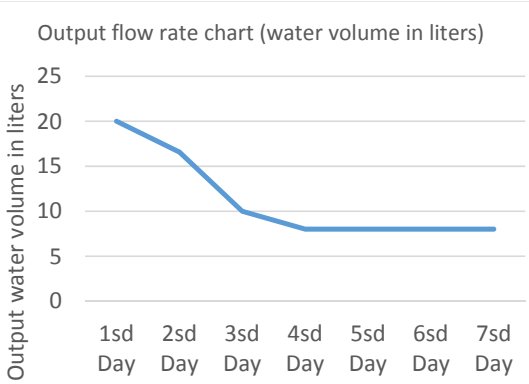

Figure 8: Outlet flow rate diagram

The graph shows high leakage in the first days of water intake and on the fourth day onwards the outlet flow rate was constant at 8 liters. The outlet flow rate of 18 samples is almost equal and since its investigation is not the subject of this thesis, we will skip its study.

Pore water pressure

Pore water pressure was investigated in each of the piezometers installed in the body and foun-

dation of the dam and the results are as shown in the table below (piezometers are in 5 rows, from top to bottom, from A to E, and the rows are named with numbers from left (upstream) to right (downstream). The pore water pressure was calculated for 18 samples, which are shown in 6 graphs with a bentonite to cement ratio of 0.1 to 0.6 below, and there are three graphs in each graph (concrete grade 150, 175, and 200). These 18 samples are for 20 piezometers in the middle of the device. The desired pressure was not present in piezometers c19, c20, and d20, so they were excluded from the study.

As shown in the diagrams above, in all the plots we are faced with pressure drop in each row and we also have pressure drop in the rows. Here it is necessary to carry out the investigation by changing the sealing walls and for each of the piezometers. (Fig. 11)

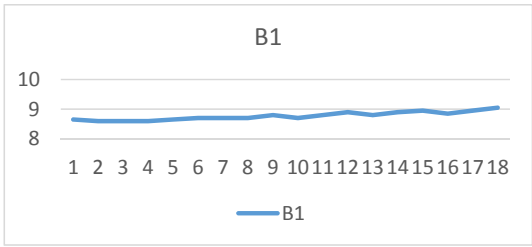

Figure 11: Diagram of pressure changes in piezometer B1 with changes in the seal walls

In the piezometer B1 diagram in samples 1, 2, and 3, the diagram is almost horizontal and no significant change is seen in it, but the general trend of the graph continues to be upward. Meanwhile, with the change in the ratio of bentonite to cement, a downward jump is observed, which is due to the decrease in cement consumption.

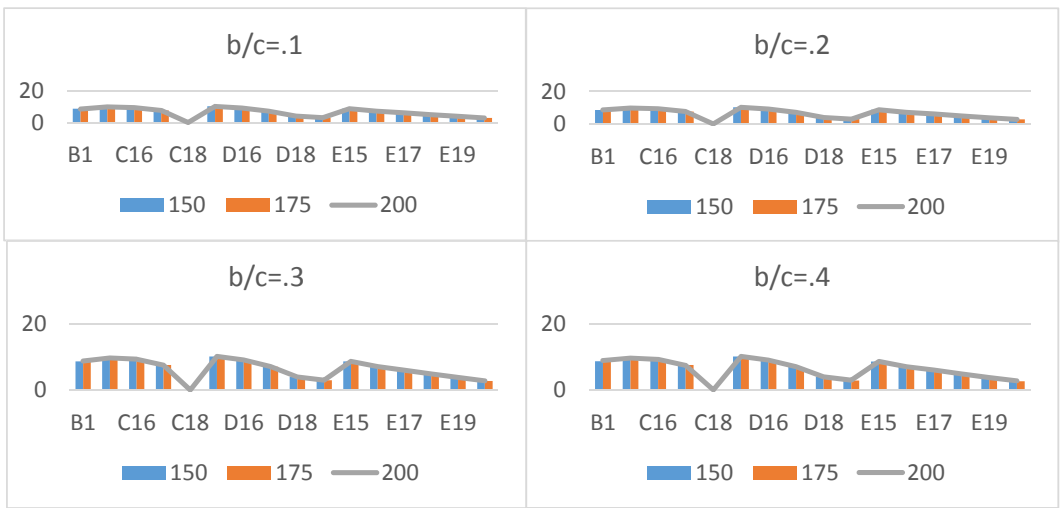

Figure 9: Pressure in piezometers at a bentonite to cement ratio of 0.5

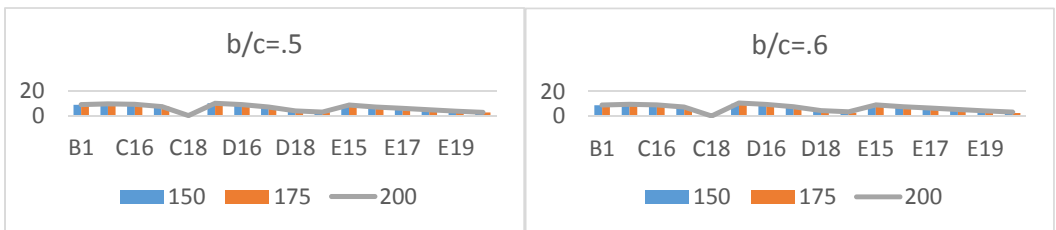

Figure 10: Pressure in piezometers at bentonite to cement ratio

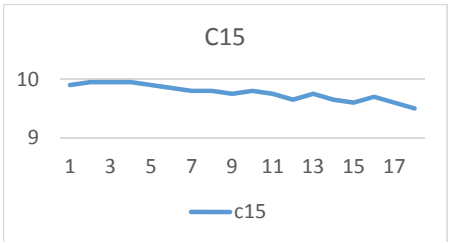

Figure 12: Diagram of pressure changes in the C15 piezometer with changes in the seal walls

In piezometer number C15 in samples 1, 2, and 3, the graph is almost horizontal and no significant change is seen in it, but the general direction of the graph continues to be downward. Meanwhile, with the change in the ratio of bentonite to cement, a downward jump is observed, which is due to the decrease in the amount of cement consumed.

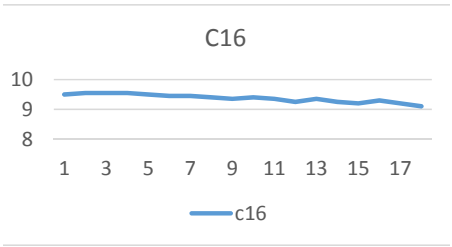

Figure 13: Diagram of pressure changes in piezometer C16 with changing seal walls

In piezometer number C16 in samples 1, 2, and 3, the graph is almost horizontal and no significant change is seen in it, but the general direction of the graph continues to be downward. Meanwhile, with the change in the ratio of bentonite to cement, a downward jump is observed, which is due to the decrease in the amount of cement consumed.

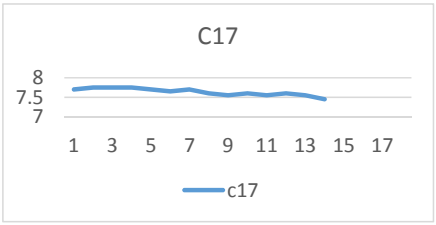

Figure 14: Diagram of pressure changes in piezometer C17 with changing seal walls

In piezometer number C17, in samples 1, 2, and 3, the graph is almost horizontal and no significant change is seen in it, but the general direction of the graph continues to be downward. Meanwhile, with the change in the ratio of bentonite to cement, a downward jump is observed, which is due to the decrease in the amount of cement consumed.

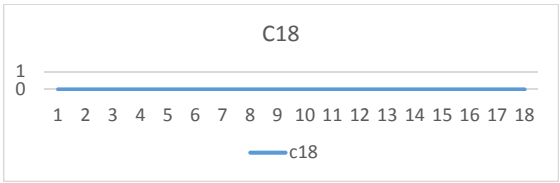

Figure 15: Diagram of pressure changes in piezometer C18 with changing seal walls

In piezometer number C18, given that this piezometer is located exactly under the dam body and behind the water wall, the flow pipes do not reach this area and the pressure in this piezometer is zero.

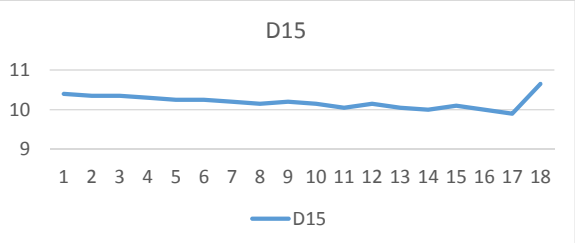

Figure 16: Diagram of pressure changes in piezometer D15 with changing seal walls

In piezometer D15, we encounter an almost constant downward trend, and in this piezometer, the last sample, which has the lowest amount of cement, had a pressure jump in the piezometer, despite the trend in the graph.

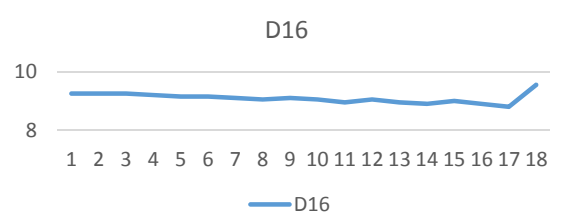

Figure 17: Diagram of pressure changes in piezometer D16 with changing seal walls

In piezometer D16, we encounter an almost constant downward trend, and in this piezometer, the last sample, which has the lowest amount of cement, had a pressure jump in the piezometer, despite the trend in the graph.

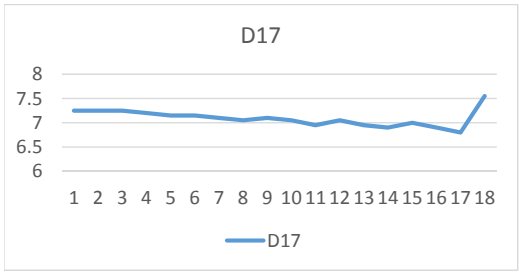

Figure 18: Diagram of pressure changes in piezometer D17 with changing seal walls

In piezometer D17, we encounter an almost constant downward trend, and in this piezometer, the last sample, which has the lowest amount of cement, had a pressure jump in the piezometer, despite the trend in the graph.

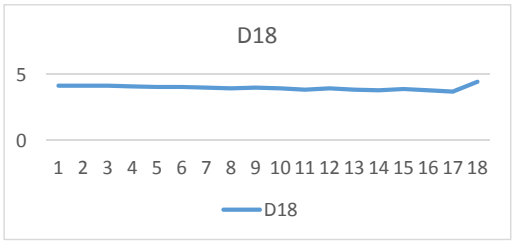

Figure 19: Diagram of pressure changes in piezometer D18 with changing seal walls

In piezometer D18, although we are facing a downward trend, the difference between the maximum and minimum is so small that the changes are not tangible. In this piezometer, the last sample, which has the lowest amount of cement, had a pressure jump in the piezometer despite the trend of the graph.

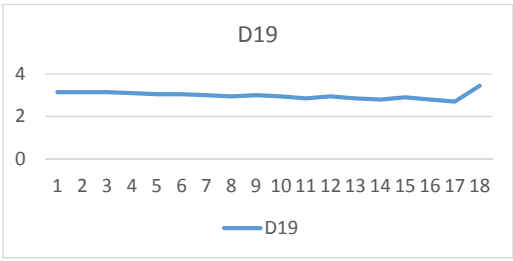

Figure 20: Diagram of pressure changes in piezometer D19 with changing seal walls

In piezometer D19, although we are facing a downward trend, the difference between the maximum and minimum is so small that the changes are not tangible. In this piezometer, the last sample, which has the lowest amount of cement, had a pressure jump in the piezometer despite the trend in the graph.

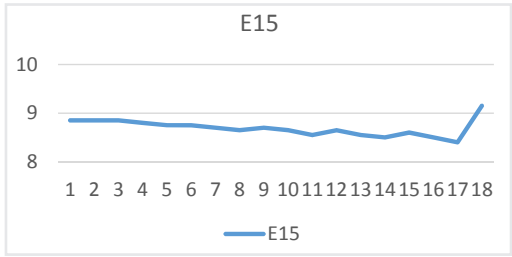

Figure 21: Diagram of pressure changes in piezometer E15 with changing seal walls

In piezometer E15, we encounter an almost constant downward trend, and in this piezometer, the last sample, which has the lowest amount of cement, had a pressure jump in the piezometer, despite the trend in the graph.

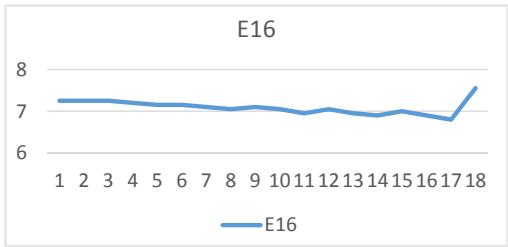

Figure 22: Diagram of pressure changes in the E16 piezometer with changes in the seal walls

In piezometer E16, we are faced with an almost constant downward trend, and in this piezometer, the last sample, which has the lowest amount of cement, had a pressure jump in the piezometer, despite the trend in the graph.

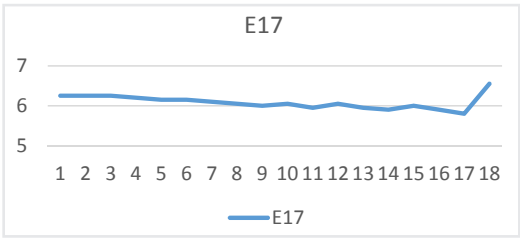

Figure 23: Diagram of pressure changes in piezometer E17 with changing seal walls

In piezometer E17, we encounter an almost constant downward trend, and in this piezometer, the last sample, which has the lowest amount of cement, had a pressure jump in the piezometer, despite the trend in the graph.

In piezometer E18, we encounter an almost constant downward trend, and in this piezometer, the last sample, which has the lowest amount of cement, had a pressure jump in the piezometer, despite the trend in the graph.

In piezometer E19, although we are facing a downward trend, the difference between the maximum and minimum is so small that the changes are not tangible. In this piezometer, the last sample, which has the lowest amount of cement, had a pressure jump in the piezometer despite the trend of the graph.

In piezometer E20, although we are facing a downward trend, the difference between the maximum and minimum is so small that the changes are not tangible. In this piezometer, the last sample, which has the lowest amount of cement, had a pressure jump in the piezometer despite the trend of the graph.

In this study, the phenomenon of seepage from the foundation of the Karkheh earthen dam was investigated using the Plaxis computational code and by studying the effect of effective parameters on the occurrence of this phenomenon. The results show that the flexibility of the dam wall was investigated based on the maximum displacement of the dam wall and without the occurrence of rupture in it, and the optimal composition of materials for one cu-

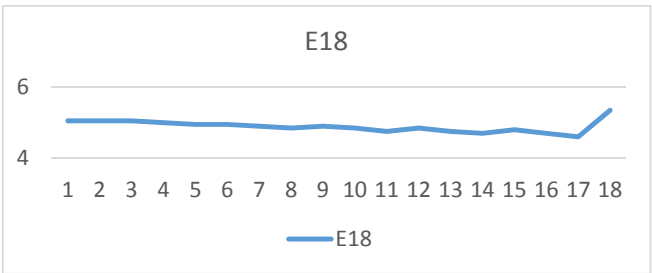

Figure 24: Diagram of pressure changes in the E18 piezometer with changes in the seal walls

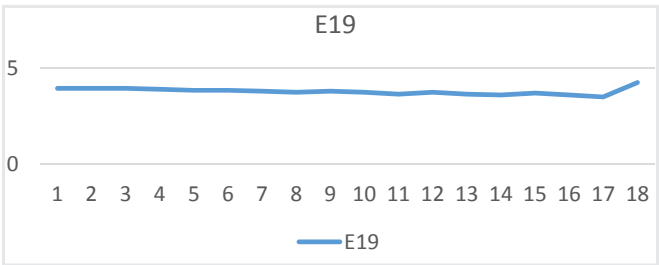

Figure 25: Diagram of pressure changes in piezometer E19 with changing seal walls

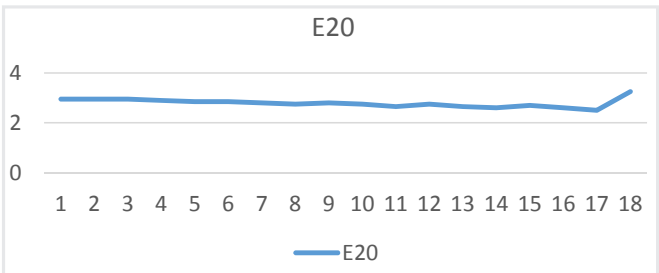

Figure 26: Diagram of pressure changes in the E20 piezometer with changing the seal walls

bic meter of concrete was proposed. In general, the results indicate that sample number 18 is not scientifically acceptable, and other technical specifications indicate and the results indicate the effect of the amount of cement, whether in the form of grade (150, 175, and 200) or in the form of the ratio of bentonite to cement from 0.1 to 0.6, showing a direct relationship between the amount of cement and the pore water pressure in the entire dam sample and the permeability of the dam wall.

REFERENCES

D'Appolonia, D.J., (1980). Soil–bentonite slurry trench cutoffs. J. Geotech. Eng. Div. 106 (4), 399–417.

Du , Y.-J.. Fan , R.-D, Krishna , Reddy , R.S. Liu , Y. Yang , Y.-L. (2015). Impacts of presence of lead contamination in clayey soil–calcium bentonite cutoff wall backfills. Applied Clay Science (108) 111–122.

Du, Y.J., Jiang, N.J., Liu, S.Y., Jin, F., Singh, D.N., Puppala, A.J., (2014a). Engineering properties and microstructural characteristics of cement-stabilized zinc-ontaminated kaolin. Can. Geotech. J. 51 (3), 289–302.

Du, Y.J., Wei, M.L., Reddy, K.R., Liu, Z.P., Jin, F., (2014b). Effect of acid rain pH on leaching behavior of cement stabilized lead-contaminated soil. J. Hazard. Mater. 271, 131– 40.

Evans, J., Ryan, C., (2005). Time-dependent strength behavior of soil–bentonite slurry wall backfill. In: Alshawabkeh, A., Benson, C.H., Culligan, P.J., Evans, J.C., Gross, B.A., Narejo, D., Reddy, K.R., Shackelford, C.D., Zornberg, J.G. (Eds.), GeoFrontiers 2005: Waste Containment and Remediation. ASCE GSP 142. ASCE, Reston, VA, pp. 1–9.

Evans, J.C., Costa, M.J., Cooley, B., (1995). The state-of-stress in soil–bentonite slurry trench cutoff walls. In: Acar, Y.N., Daniel, D.E. (Eds.), Geoenvironment 2000: Characterization, Containment, Remediation, and Performance in Environmental Geotechnics. ASCE GSP 46. ASCE, Reston, VA, pp. 1173–1191.

Fan, R.D., Du, Y.J., Chen, Z.B., Liu, S.Y., (2013). Engineering behavior and sedimentation behavior of lead contaminated soil–bentonite cutoff wall backfills. J. Cent. South Univ. 20 (11), 2255–2262.

Fan, R.D., Du, Y.J., Liu, S.Y., Chen, Z.B., (2014b). Compressibility and hydraulic conductivity of sand/clay–bentonite backfills. In: Reddy, K.R., Shen, S.J. (Eds.), Geo-Shanghai 2014: Geoenvironmental Engineering. ASCE GSP 241. ASCE, Reston, VA, pp. 21–30.

Grim, R.E., (1968). Clay Mineralogy. 2nd ed. McGraw Hill, New York.

Hong, Z.S., Zeng, L.L., Cui, Y.J., Cai, Y.Q., Lin, C., (2012). Compression behaviour of natural and reconstituted clays. Geotechnique 62 (4), 291–301.

Horpibulsuk, S., Shibuya, S., Fuenkajorn, K., Katkan, W., (2007). Assessment of engineering properties of Bangkok clay. Can. Geotech. J. 44 (2), 173–187.

Hu, L., Wu, X., Liu, Y.,Meegoda, J.N., Gao, S., (2010). Physical modeling of air flow during air sparging remediation. Environ. Sci. Technol. 44 (10), 3883–3888.

Li, Z., Katsumi, T., Inui, T., Takai, A., (2013b). Fabric effect on hydraulic conductivity of kaolin under different chemical and biochemical conditions. Soils Found. 53 (5), 680–691.

Malusis, M.A., Barben, E.J., Evans, J.C., (2009). Hydraulic conductivity and compressibility of soil–bentonite backfill amended with activated carbon. J. Geotech. Geoenviron. Eng. ASCE 135 (5), 664–672.

Malusis, M.A., McKeehan, M.D., (2013). Chemical compatibility of model soil–bentonite backfill containing multiswellable bentonite. J. Geotech. Geoenviron. Eng. ASCE 139 (2), 189–198.

Mishra, A.K., Ohtsubo, M., Li, L.Y., Higashi, T., Park, J., (2009). Effect of salt of various concentrations on liquid limit, and hydraulic conductivity of different soil–bentonite mixtures. Environ. Geol. 57 (5), 1145–1153.

Mitchell, J.K., Soga, K., (2005). Fundamentals of Soil Behavior. 3rd ed. JohnWiley and Sons Inc., New York, NY.

Rahimi, H. (2010),"Embankment Dams," University of Tehran press, Iran, 671pp.

Ruffing, D.G., Evans, J.C., Malusis, M.A., (2010). Prediction of earth pressures in soil– bentonite cutoff walls. In: Fratta, D.O., Puppala, A.J., Muhunthan, B. (Eds.), GeoFlorida (2010): Advances in Analysis, Modeling and Design. ASCE GSP 199. ASCE, Reston, VA, pp. 2416–2425.

Sharma, H.D., Reddy, K.R., (2004). Geoenvironmental Engineering: Site Remediation,Waste Containment, and Emerging Waste Management Technologies. JohnWiley and Sons Inc., New York.

Sivapullaiah, P., Sridharan, A., Stalin, V., (2000). Hydraulic conductivity of bentonite–sand mixtures. Can. Geotech. J. 37 (2), 406–413.

Taylor, D.W., (1948). Fundamentals of Soil Mechanics. John Wiley & Sons Inc., New York.

Xu, Y.S., Ma, L., Shen, S.L., Sun, W.J., (2012). Evaluation of land subsidence by considering underground structures that penetrate the aquifers of Shanghai, China. Hydrogeol. J. 20 (8), 1623–1634.

Xue, Q., Li, J.S., Liu, L., (2013). Experimental study on anti-seepage grout made of leachate contaminated clay in landfill. Appl. Clay Sci. 80–81, 438–442.

Yong, R.N., Ouhadi, V.R., Goodarzi, A.R., (2009). Effect of Cu2+ ions and buffering capacity on smectite microstructure and performance. J. Geotech. Geoenviron. Eng. ASCE 135 (12), 1981–1985.

Yukselen-Aksoy, Y., Kaya, A., Ören, A.H., (2008). Seawater effect on consistency limits and compressibility characteristics of clays. Eng. Geol. 102 (1–2), 54–61.

HOW TO CITE THIS ARTICLE
Mahbod, A. , Saba, H. R. , Yousefi Rad, M. and Lajvardi, H. (2024). Construction of a device for laboratory investigation of seepage specifications different states of the Karkheh dam damwall. International Journal of Urban Management and Energy Sustainability, (), -.
DOI: 10.22034/ijumes.2024.2043838.1263